IBRACON Structures and Materials Journal
Revista IBRACON de Estruturas e Materiais

ORIGINAL ARTICLE

Load transfer on instrumented prestressed ground anchors in sandy soil

Transferência de carga em ancoragens protendidas instrumentadas em solo arenoso

Alex Micael Dantas de Sousa[a] (iD)
Yuri Daniel Jatobá Costa[b] (iD)
Luiz Augusto da Silva Florêncio[c] (iD)
Carina Maria Lins Costa[b] (iD)

[a]Universidade de São Paulo – USP, Escola de Engenharia de São Carlos, Departamento de Engenharia de Estruturas, São Carlos, SP, Brasil
[b]Universidade Federal do Rio Grande do Norte – UFRN, Departamento de Engenharia Civil, Natal, RN, Brasil
[c]Universidade Federal do Rio de Janeiro – UFRJ, Departamento de Engenharia Civil, Rio de Janeiro, RJ, Brasil

Abstract: This study evaluates load variations in instrumented prestressed ground anchors installed in a bored pile retaining wall system in sandy soil. Data were collected from instrumentation assembled in the bonded length of three anchors, which were monitored during pullout tests and during different construction phases of the retaining wall system. Instrumentation consisted of electrical resistance strain gauges positioned in five different sections along the bonded length. Skin friction distributions were obtained from the field load measurements. Results showed that the skin friction followed a non-uniform distribution along the anchor bonded length. The mobilized skin friction concentrated more intensely on the bonded length half closest to the unbonded length, while the other half of the bonded length developed very small skin friction. The contribution of the unbonded length skin friction to the overall anchor capacity was significant and this should be accounted for in the interpretation of routine anchor testing results. Displacements applied to the anchor head were sufficient to mobilize the ultimate skin friction on the unbonded length, but not on the bonded length. Performance of loading-unloading stages on the ground anchor intensified the transfer of load from the unbonded length to the bonded length. Long-term monitoring of the anchor after lock-off revealed that the load at the anchor bonded length followed a tendency to reduce with time and was not significantly influenced by the retaining wall construction phases.

Keywords: ground anchor, load transfer, skin friction, retaining wall, bored pile.

Resumo: O presente estudo avalia as variações de carga em ancoragens protendidas instrumentadas, instaladas em uma estrutura de contenção composta por estacas escavadas em solo arenoso. Os dados foram coletados a partir de instrumentação disposta no trecho ancorado de três ancoragens, monitoradas durante ensaios de arrancamento e durante diferentes etapas construtivas da contenção. As ancoragens foram instrumentadas com extensômetros elétricos de resistência em cinco seções distintas posicionadas ao longo do trecho ancorado. Distribuições de atrito lateral foram obtidas a partir das medições de carga em campo. Os resultados revelaram uma distribuição não uniforme do atrito lateral ao longo do trecho ancorado. O atrito lateral mobilizado concentrou-se mais intensamente na metade do trecho ancorado mais próxima ao trecho livre, ao passo que uma parcela muito pequena de atrito lateral foi mobilizada na outra metade do trecho ancorado. A contribuição do atrito lateral no trecho livre para a capacidade de carga da ancoragem foi significativa, o que deve ser levado em consideração na interpretação dos resultados de ensaios de rotina em tirantes. Os deslocamentos aplicados na cabeça da ancoragem foram suficientes para mobilizar o atrito lateral último no trecho livre, porém não no trecho ancorado. A execução de estágios de carga-descarga na ancoragem contribuiu para intensificar a transferência de carga do trecho livre ao trecho ancorado. O monitoramento de longo-prazo da ancoragem após incorporação do carregamento revelou que a carga no trecho ancorado seguiu uma tendência de redução ao longo do tempo, não tendo sido significativamente influenciada pelas etapas construtivas da contenção.

A. M. D. Sousa, Y. D. J. Costa, L. A. S. Florêncio, and C. M. L. Costa

1 INTRODUCTION

Prestressed bond-type grouted anchors are structural elements in which the load is transferred to the ground from a steel tendon bonded to grout. The design of ground anchors can be based on field load tests [1], [2], semi-empirical models [3], [4] and numerical models [5], [6]. Most usual solutions for the design of the bonded length of ground anchors consist of semi-empirical methods [3]–[7], [8]. Although practical for routine applications, semi-empirical methods lose accuracy beyond their range of calibration, which can result in uneconomical design projects due to the high safety factors required to balance the uncertainties and errors involved.

A way to boost the growth of more rational semi-empirical methods for prestressed ground anchor design is to encourage studies involving monitoring of ground anchors in the field. However, most publications to date on stabilized slopes and excavations have focused on soil-nailing systems by developing reduced-scale physical models and numerical studies [9], [10]. A limited number of publications on the behavior of prestressed ground anchor in the field is available. Among the scarcely documented investigations, just a few include results from instrumented ground anchors [5], [6], [11]–[13]. Most available studies involve anchors in clayey soils [14]–[16] and rocks [17]–[19], while anchors in granular soils are more unusual.

Additionally, while ground anchor monitoring has typically focused on the total applied load on the anchor head, investigations on load variations along the anchor bonded length have been virtually overlooked. Particularly, improvement of design solutions for ground anchors can be achieved by assessing load and skin friction variations along the anchor's bonded and unbonded lengths in the field [3]–[7], [20], [21].

The purpose of this paper is to evaluate the load-transfer behavior of prestressed ground anchors installed in a retaining wall system composed of spaced bored piles in a sandy soil profile. Data were collected from the instrumented bonded length of three anchors, both during pullout tests and during different construction phases of the retaining wall. The contribution of the anchor unbonded length to the anchor bearing capacity and the variations of load on the anchor bonded length are evaluated. Skin friction values estimated from the field results are compared to values obtained from theoretical methods.

2 BACKGROUND

2.1 Brief description of design methods for ground anchor pullout capacity estimation

Empirical and semi-empirical methods for estimating the ultimate pullout capacity of ground anchors are abundant in the literature. Ostermayer [3] proposed a solution that includes the use of empirical design charts elaborated from the results of approximately 300 field tests in anchors, carried out in Germany. The proposed charts relate the anchor bonded length to the ultimate load capacity or the ultimate skin friction. The grout injection pressure used during the installation of the anchors in the field is not reported.

Bustamante and Doix [22] developed a design method that accounts for the installation process, the grout injection pressure in single or multiple phases, and the volume of injected grout. The anchor ultimate pullout capacity is estimated by considering a coefficient β that accounts for the diameter increase of the bonded length due to grout injection pressure. Values for β are given for different soil types and for single-phase or double-phase grout injection procedures. The ultimate skin friction on the anchor bonded length is estimated from empirical design charts devised for cohesive and cohesionless soils, which take into consideration whether grouting is performed in single or multiple injection stages. However, it is worth mentioning that the anchor failure load was not reached in most experiments used to create the method.

Costa Nunes [7] proposed a formulation similar to that of Bustamante and Doix [22], but assuming that failure at the ground-grout interface is governed by the Mohr-Coulomb failure theory. The ultimate anchor capacity for anchors is given by:

$$T_{max} = \pi \cdot D_e \cdot L_b \cdot \left[c' + (\gamma \cdot h + p) \cdot tan' \right] \tag{1}$$

where: D_e is the average diameter of the ground anchor section; L_b is the anchor bonded length; c' is the soil-grout adhesion; γ is the specific unit weight of the soil at the depth of the anchor bonded length middle span; h is the depth of the anchor bonded length middle span; ϕ' is the internal friction angle of the soil; Δp is the increase in the vertical stress due to the residual injection pressure. Costa Nunes [7] suggests assuming Δp between $5\gamma h$ and $10\gamma h$. The ultimate skin friction is given by the term between brackets in Equation 1.

AASHTO [23] recommends a method for calculating the pullout resistance of anchors in cohesive soils, cohesionless soils and rocks. Proposed values for the ultimate skin friction for cohesionless soils take into consideration soil type, soil compactness and grout injection pressure. It is advised that the presumptive ultimate skin friction values offered by the method are intended for preliminary design or evaluation of the feasibility of straight shaft anchors installed in small diameter boreholes. Therefore, conservative design pullout capacities can result from using these values.

The former version of Brazilian code ABNT NBR 5629 [24] suggests a method for calculating the pullout capacity of anchors embedded in cohesive and cohesionless soils, which is analogous to that proposed by the current version of the Canadian Foundation Engineering Manual [25]. For cohesionless soils, the ultimate skin friction is given by the product of the overburden vertical stress at the middle span of the bonded length and the skin friction coefficient (k_f). Values for k_f are provided according to soil compactness and soil type (silts, fine sands, medium sands, and coarse sands). The effect of grout injection pressure on pullout capacity is disregarded in the method. No specific method for pullout capacity prediction of ground anchors is proposed by the current version of the Brazilian standard ABNT NBR 5629 [26].

2.2 Load transfer evaluation from ground anchor monitoring

Contrary to what is assumed in most proposed design solutions for ground anchors, the mobilized interface skin friction was found to behave non-uniformly along the anchor bonded length [27], [28]. One reason for the non-uniformity is the dependency of the skin friction on the relative displacement (δ) between the grout body and the surrounding soil [27], [29], [30]. The skin friction reaches the peak value (f_{ult}) and then reduces with increasing relative displacements (δ), until reaching the residual value (f_r). As the load applied to the anchor head is increased, the peak skin friction progressively moves from the portion of the bonded anchor length that is closest to the unbonded length towards the bonded length end. According to Barley and Windsor [31], typically, a ground anchor with a bonded length of 6 m needs, at proof load, to displace about 15 to 20 mm at the top end of the bonded length before any load is transferred to its bottom end.

Selection of an appropriate design value for the soil-grout interface skin friction from design manuals and codes is highly subjective [18]. Capturing the load transfer mechanisms that take place in the anchor bonded length in the field is essential for improving design methodologies. However, while the relationship between the applied load and the anchor head displacement can be easily assessed from standard pullout tests, the load distribution along the bonded length requires a more complex apparatus, which makes it difficult to be obtained in ordinary circumstances.

Li et al. [15] presented one of the first studies on the load transfer of ground anchors. Electrical resistance strain gauges were installed along the anchor bonded length. The anchors were used to stabilize a diaphragm retaining wall on a soil profile consisting of silt and clay layers. The anchors were constructed with a length of 30 m (of which 23 m corresponded to the bonded length). It was observed, from the instrumentation, that the load was not distributed linearly along the bonded length, but concentrated more at its beginning. The load was found to be virtually zero between the middle span and the end of the bonded length.

Briaud et al. [16] investigated variations of load in the bonded length of anchors embedded in a clay soil using vibrating wire extensometers. The instrumented anchors had a bonded length of 4.6 m and a total length of 13.8 m. Results revealed a load distribution configuration similar to that identified by Li et al. [15], that is, a higher concentration of load at the beginning of the anchor's bonded length.

Iten and Puzrin [27] used fiber optic sensors to investigate the load-transfer in 8-m long anchors. It was observed that the load followed a non-linear distribution, with a drastic reduction at the last 2 m of the bonded length.

Bryson and Giraldo [18] analyzed instrumented ground anchors constructed for a landslide stabilization system in a shale stratum. Load transfer was studied based on strain gauge measurements along the bonded length of the anchors, which measured 4.6 m. The strain gauge monitoring revealed that some slippage occurred between the tendon and the grout. The slippage increased as the anchor head load increased. Only minor variations in the strain gauge data were observed after the construction period and during the long-term monitoring, suggesting that the anchor bonded length reached equilibrium and that the anchors installed in the shale stratum did not show significant creep susceptibility.

Platzer et al. [32] conducted a study focusing on the compressive behavior of piles and tensile behavior of ground anchors embedded in cohesionless soils and subjected to dynamic loading. The bonded length of the anchors measured 5.1 m and was instrumented with four strain-gauge sections. The authors observed that the dynamic tensile force distribution along the anchors decreases nonlinearly with increasing anchor length. Moreover, the authors identified that the dynamic tensile forces were depleted within a shorter distance in the anchor than the static tensile forces.

3 RETAINING WALL DESCRIPTION AND SUBSOIL CHARACTERISTICS

3.1 Retaining wall description

A schematic of the elevation view of the retaining wall analyzed in this investigation is shown in Figure 1. The retaining wall had a total height of 8.95 m, a length of 56 m and was built with spaced bored piles with 300 mm in diameter and 14.85 m in length. The piles were installed in the ground with a spacing between axes of 350 mm. The characteristic concrete compressive strength of the piles at 28 days was 25 MPa. The pile reinforcement consisted of 11 longitudinal bars with 10 mm in diameter and 12 m in length, enveloped by a coil steel spiral with 5 mm in diameter and 100 mm in spacing. The top of the piles was connected to a head beam with cross section dimensions of 400 mm x 650 mm.

Figure 1 - Schematic showing front elevation view of the instrumented retaining wall (units: m).

The retaining wall was anchored by two rows of ground anchors constructed with steel threaded bar tendons with 32 mm in diameter and installed in a borehole with 100 mm in diameter (D_b). Uniaxial tensile tests were performed on the tendons in order to obtain the elastic modulus. Table 1 lists the mechanical properties of the used bar tendons.

Table 1 - Characteristics of the bar tendons.

Diameter (mm)	32
Yield stress (MPa)	950
Tensile strength (MPa)	1,050
Yield load (KN)	760
Ultimate load (KN)	840
Elastic modulus (MPa)	205,000
Cross-sectional area (mm^2)	804

The horizontal spacing between anchor axes was 2.75 m for the anchors of the upper row and 1.75 m for the anchors of the lower row (Figure 1). Figure 2a shows a cross-section view of the retaining wall, with the position of the anchor rows in relation to the excavation ground surface and the dimensions of the anchor bonded and unbonded lengths. The anchors of the upper row had a bonded length of 8 m and an unbonded length of 6 m, while the anchors of the lower

A. M. D. Sousa, Y. D. J. Costa, L. A. S. Florêncio, and C. M. L. Costa

row had a bonded length of 9 m and an unbonded length of 5 m. A detail of the assembly of the anchor in the bonded length is shown in Figure 2b. Design tensile loads of 192 kN and 260 kN were calculated for the upper and lower rows, respectively. Both rows had the anchor heads connected to a beam with dimensions of 400 mm x 700 mm.

(1) - Borehole (100 mm in diameter)
(2) - Bar tendon (32 mm in diameter)
(3) - Cement grouting
(4) - Centralizer (2 m in spacing)
(5) - Injection tube (25 mm in diameter)

(a)   (b)

Figure 2 - (a) Schematic showing the cross-section view of the retaining wall system (units: m); (b) detail of the anchor assembly in the bonded length.

Grouting injection was performed in two steps. In the first step, cement grout was injected with a water/cement ratio of approximately 0.5. After the curing of grout in the first injection step, a second injection step with a cement grout with a water/cement ratio of approximately 0.6 was carried out to fill the borehole. Grout was injected in the bonded length with a pressure of 1500 kPa. The unbonded length of the anchor was protected with a PVC debonding sleeve.

Figure 3 shows the building phases of the retaining wall system. Initially, the bored piles were cast in the ground (phase 1). Then, the soil was excavated to a depth of 2.7 m from ground level (phase 2) and the upper row of anchors was installed (phase 3). A new excavation phase was carried out to a depth of 5.65 m (phase 4) and the lower row of anchors was installed (phase 5). The excavation was finished at a depth of 8.12 m (phase 6). The effect of the construction phases on anchor behavior was assessed during the monitoring of the ground anchors. The lateral displacements of the retaining wall were monitored with an inclinometer during the building phases [13], and were less than 0.1% of the excavation height.
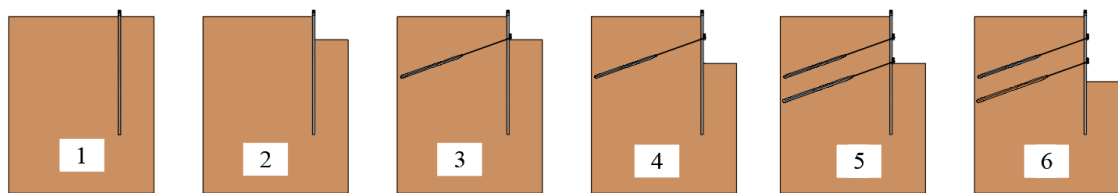
Figure 3 - Retaining wall building phases.

3.2 Subsoil characteristics

The constructed retaining wall is located in the City of Natal, Brazil. Field survey included standard penetration tests (SPT) at two different locations, identified in this study as SP01 and SP02. The tests were performed according to ABNT NBR 6484 [33] and were located near the crest of the excavation, 15.5 m apart from each other. Figure 4a shows the soil stratification at the site and Figure 4b shows the variation of the N_{SPT} blow-count resistance corrected for 60% efficiency (N_{60}) with depth and corresponding mean values. Corrections of the N_{SPT} values were carried out by assuming an efficiency of 72% for the tests, as mentioned by Décourt et al. [34] regarding the Brazilian practice. The soil profile is composed of fine sand and slightly clayey fine sand layers overlying a stiff sandy clay layer, where the tip of the

piles rest. The classification of the soil layers according to the Unified Soil Classification System (USCS) is given in Figure 4a.
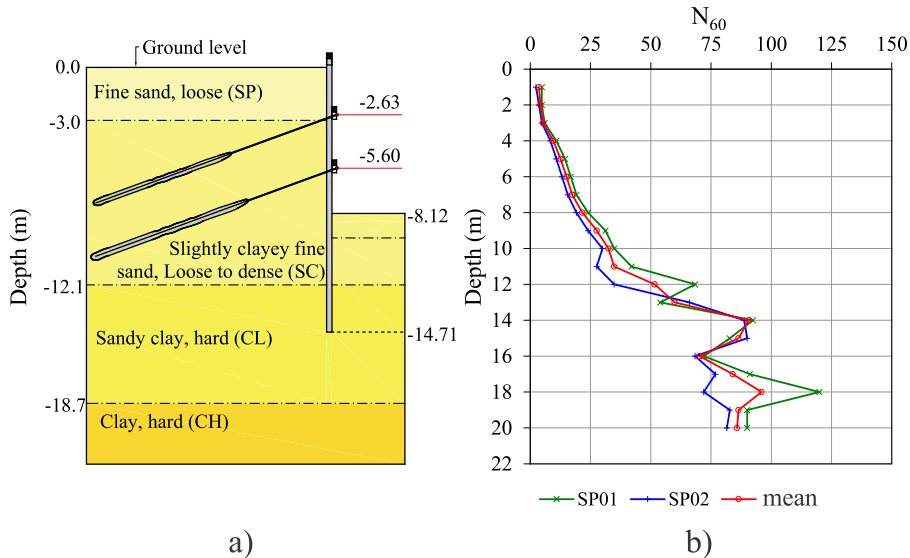
Figure 4 - (a) Subsoil profile (units: m); (b) N_{60} blow-count resistance with depth.

The grain size distribution of the slightly clayey fine sand, where the bonded length of the upper and bottom rows is installed, is shown in Figure 5. The slightly clayey fine sand has an average particle size of 0.22 mm (24.2% of particles are finer than 0.075 mm and more than 99.3% of particles are finer than 2 mm). The specific gravity of this soil is 2.65.
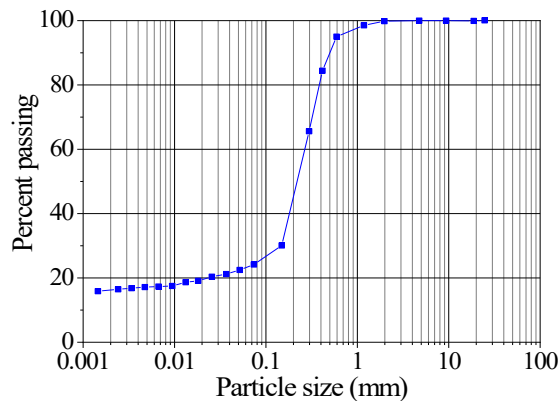
Figure 5 - Grain-size distribution of the slightly clayey fine sand.

Shear strength parameters of the slightly clayey fine sand were obtained from one series of conventional CID triaxial compression tests carried out with confining effective stresses (σ'_3) of 50 kPa, 100 kPa, and 200 kPa. Specimens were prepared with a specific unit weight of 17 kN/m³ to represent field conditions. The results of deviator stress-axial strain behavior for the soil are presented in Figure 6a, and the corresponding *p-q* diagram is presented in Figure 6b. The peak friction angle (ϕ'_p) of the soil equals 31° and was obtained from the inclination of the K_f line shown in Figure 6b.

Rev. IBRACON Estrut. Mater., vol. 14, no. 6, e14612, 2021

6/19
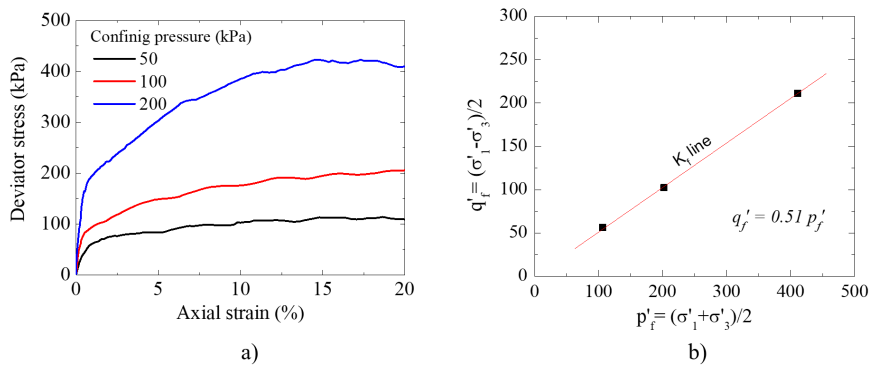
Figure 6 - Results of CID triaxial tests performed on the slightly clayey fine sand: a) Deviator stress v. axial strain relationships for varying confining pressures; b) *p-q* diagram.

3.3 Ground anchor instrumentation

Three anchors of the retaining wall were instrumented with electrical resistance foil strain gauges to monitor the axial force along the anchor bonded length (labeled as T10, T33 and T36, as shown in Figure 1). Double rosette model strain gauges with a nominal resistance of 120 Ω, connected in a full Wheatstone bridge circuit, were used in the instrumentation of five sections along the bonded length of each anchor. An illustration of the instrumented ground anchors is presented in Figure 7. Table 2 displays the distances of the instrumented sections from the bonded length beginning (L_{se}) in the three ground anchors. The instrumented sections are labeled as SG1 to SG5. The first instrumented section (SG1) of each ground anchor was positioned as close as possible from the beginning of the bonded length. Sections SG1 and SG4 of anchor T10 and section SG2 of anchor T33 presented malfunction after installation of the anchor and were unable to generate data during the tests. Figure 8a shows a stack of bar tendons that were used in the anchors of the retaining wall system. A detail of one instrumented bar tendon is shown in Figure 8b.
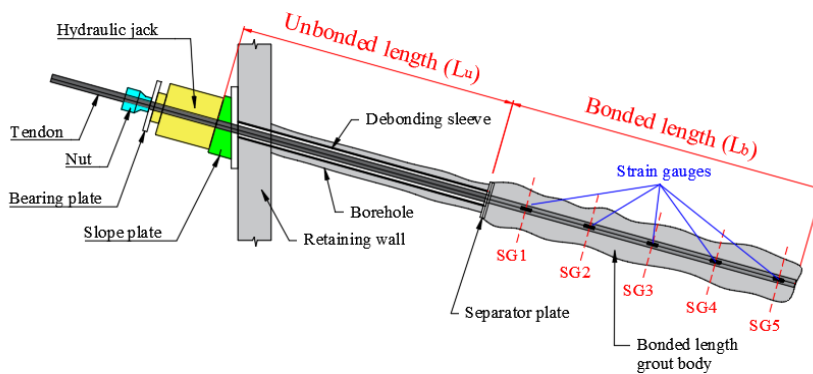
Figure 7 - Instrumented ground anchor.

Table 2 - Positions of the instrumented sections in the anchor bonded length.

Anchor	L_u (m)	L_b (m)	L_{se} (m)				
			SG1	SG2	SG3	SG4	SG5
T10	6.00	9.50	1.65	3.50	5.35	7.20	9.25
T33	5.00	9.25	0.70	1.20	3.35	5.50	9.00
T36	5.00	9.50	0.65	1.20	3.40	5.60	9.25

Note: L_u = anchor unbonded length; L_b = anchor bonded length; L_{se} = distance from the beginning of the bonded length to the instrumented section.

Rev. IBRACON Estrut. Mater., vol. 14, no. 6, e14612, 2021

7/19
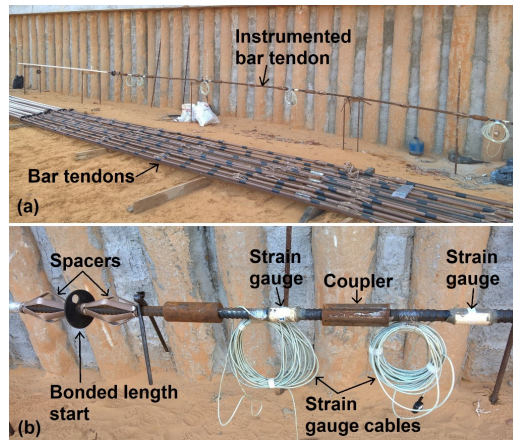
Figure 8 - (a) Bar tendons used in the field; (b) Detail of an instrumented bar tendon.

3.4 Pullout test description

The pullout tests were carried out according to Brazilian code ABNT NBR 5629 [26]. The tensile load was applied by a hydraulic jack with a maximum nominal capacity of 500 kN, connected to a manual pump reacting against the external retaining wall face. The load was applied in cumulative equal increments until stabilization. Displacements of the tendon were recorded at the anchor head using a dial gauge with a resolution of 0.01 mm and a maximum stroke of 50 mm. The dial gauge was fixed in place by a magnetic-articulated base mounted on a steady reference beam. The pullout test apparatus is shown in Figure 9. During the pullout tests and construction phases of the retaining wall, data from the instrumented sections and the load cell were recorded at predetermined time intervals with a data acquisition system with eight channels for strain-gauge-based transducers, manufactured by HBM B.V., model Spider8.

The acceptance tests on anchors T10, T33 and T36 were carried out with a single loading-unloading stage. The acceptance tests started with an initial load (F_0) calculated as $0.1f_{yk}A$ (where f_{yk} is the characteristic tensile strength of the tendon and A is the tendon cross-sectional area). After reaching the maximum load (F_{max}), the anchor was unloaded to F_0, reloaded to the design load (F_d), and then locked-off.
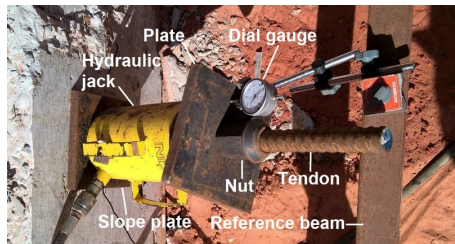
Figure 9 - Pullout test apparatus.

The suitability test on anchor T33 was conducted with four loading-unloading stages. Target loads for the load steps of the suitability test were F_0, $0.5F_d$, $1F_d$, $1.25F_d$, $1.5F_d$ and $2F_d$. After the conclusion of the test, the anchor was completely unloaded. The pullout tests were conducted at least 15 days after the installation of the ground anchor, allowing enough time for grout curing. Table 3 summarizes the characteristics of the pullout tests performed on the instrumented ground anchors.

Table 3 - Pullout test characteristics.

Ground anchor	Test type	L_u (m)	L_b (m)	h_b (m)	F_d (kN)	F_{max} (kN)
T10	Acceptance	6.00	9.50	6.16	200	360
T33	Acceptance	5.00	9.25	8.95	260	400
T33	Suitability	5.00	9.25	8.95	260	495
T36	Acceptance	5.00	9.50	8.95	260	400

In Table 3, L_u is the anchor unbonded length, L_b is the anchor bonded length, h_b is the depth of the bonded length at its middle span, F_d is the ground anchor design load and F_{max} is the maximum load reached in the test.

4 RESULTS

4.1 Pullout test results

Figure 10a shows the load-displacement curve obtained with the suitability test performed on ground anchor T33. The applied loading-unloading stages allowed separation between elastic (d_e) and plastic (d_p) components of the total displacement measured at the anchor head, as shown in Figure 10b. The anchor unbonded length (L_u) was predicted from Equation 1 [24]:

$$L_u = \frac{\Delta d_e}{\Delta F} EA \tag{1}$$

where: Δd_e is the elastic displacement variation and ΔF is the pullout load variation.

Equation 1 resulted in an unbonded length equal to 5.6 m, which is slightly larger than the unbonded length of 5 m constructed in the field (see Table 3).

Following the procedure described in ABNT NBR 5629 [26], the load reduction due to skin friction along the anchor unbonded length was estimated as the difference between points A and B in the horizontal axis of Figure 10b. Specifically, point B is defined as the intersection between the horizontal axis and a straight line fitted to the elastic displacement curve. A load reduction equal to 60 kN, which corresponds to about 12% of the maximum applied load (F_{max} = 495 kN), was obtained according to this procedure.
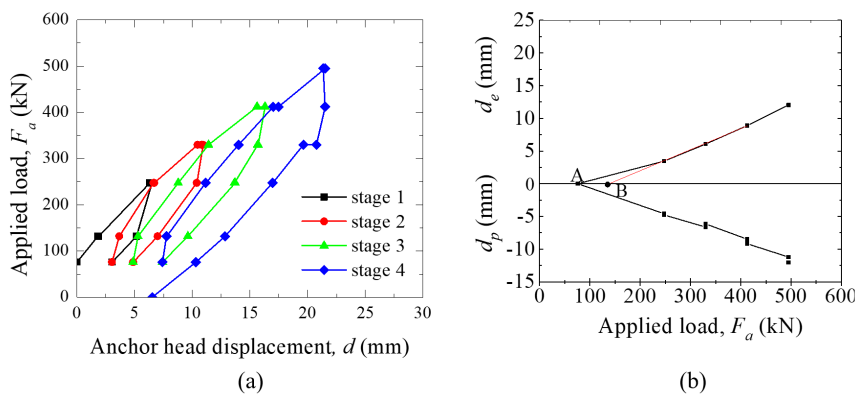
Figure 10 - Suitability test results of anchor T33: (a) Applied load v. anchor head displacement; (b) elastic and plastic displacements.
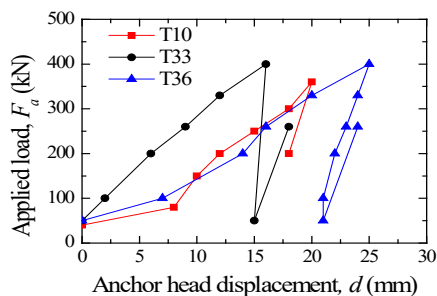
Figure 11 - Acceptance test results of anchors T10, T33 and T36.

Figure 11 shows the load-displacement curves obtained from the acceptance tests on anchors T10, T33 and T36. The head displacement (d) of anchors T10 and T36 was significantly large at the first load increment. This important initial movement of the anchor head might have been a result of soil disturbance during borehole excavation, as well as a consequence of the bentonite-based mud used for stabilizing the borehole during drilling and anchor installation. Significant initial movements in tensile load tests in anchor elements have been reported elsewhere [35], [36]. Due to the previous suitability test, only small displacements developed on anchor T33 during the acceptance test. This increase in the stiffness response of anchor T33 can be attributed to the improvement of the interface shear strength (skin friction) on the bonded length after the previous loading-unloading sequences in the suitability test (Section 3.4). This phenomenon has also been identified by Platzer et al. [32].

4.2 Load distribution on anchor bonded length

Figure 12a, c shows the measured load (F_m) at the instrumented sections of anchors T10 and T36, respectively, as a function of the distance of the instrumented section from the bonded length start normalized by the anchor bonded length (L_{se}/L_b). Figure 12b, d show F_m normalized by the load applied at the anchor head (F_a) as a function of L_{se}/L_b. Data from instrumented sections SG1 and SG4 of anchor T10 and section SG2 of anchor T33 are not included in this analysis because these sections have been damaged during anchor installation, as previously reported.
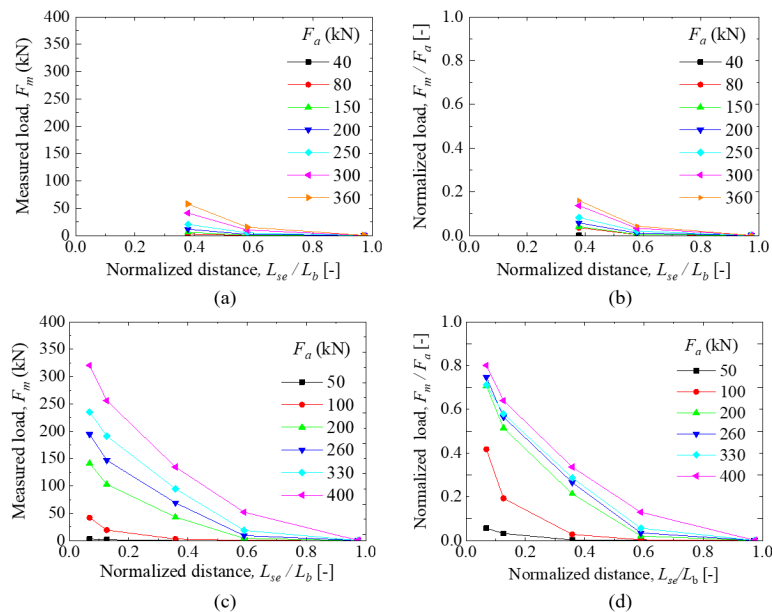
Figure 12 - Load distribution on bonded length of anchors T10 and T36: (a) Anchor T10: measured load v. normalized distance; (b) Anchor T10: normalized load v. normalized distance; (c) Anchor T36: measured load v. normalized distance; (d) Anchor T36: normalized load v. normalized distance.

The experimental results show that the load concentrated more at the beginning of the anchor bonded length and dropped with increasing distance [15], [16], [28]. The degradation of the measured load (F_m) is more significant at higher F_a levels. As the load applied to the anchor head increases, the load at the unbonded length is gradually transferred to the bonded length. In both anchors T10 and T36, the load reaching the farthest half of the bonded length was smaller than 20% of the load applied at the anchor head, while the load reaching the farthest instrumented section (SG5) was negligible.

Figure 13 presents the load distribution on the bonded length of anchor T33. Normalized measured load (F_m/F_a) versus normalized distance (L_{se}/L_b) relationships are shown for all loading stages carried out in the suitability test performed on anchor T33. Similar to anchors T10 and T36, the load concentrates more at the region closest to the beginning of the bonded length [15], [16], [28]. It is also observed that the normalized load becomes very reduced beyond a distance equal to approximately $L_{se}/L_b = 0.4$, which means that most of the load is supported by the first half of the anchor bonded length.
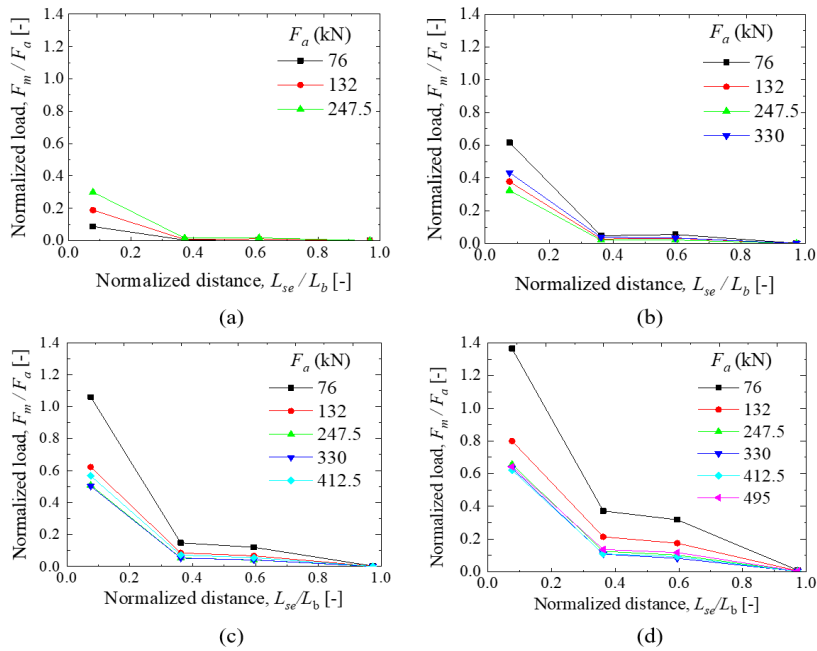
Figure 13 - Load distribution on bonded length of anchor T33 during the suitability test: (a) 1st loading stage; (b) 2nd loading stage; (c) 3rd loading stage; (d) 4th loading stage.

Figure 14 compares the load applied to the anchor head (F_a) with the corresponding measured load (F_m) at section SG1 of anchor T33. The same applied load resulted in a higher measured load in each new stage, as a consequence of the build-up of residual load at the bonded length after unloading to F_a = 76 kN in each stage. The load build-up is caused by the recovery of a portion of the elastic elongation of the tendon's unbonded length after unloading. It can be noted that the residual load increment (ΔF_m) was reduced from stage to stage. Specifically, ΔF_m virtually vanished in stage 4.

Figure 14 also reveals that the measured load at SG1 remained unchanged at the beginning of the loading path of stages 2 to 4, and just increased with the applied load for F_a values higher than 132 kN. This behavior can be attributed to the mobilized skin friction on the anchor's unbonded length, which is initially high enough to prevent any change in the measured load at SG1, but recedes after some anchor displacement [28]. The average load-transfer rate in the loading phase of each stage can be assessed from the inclination of the dashed lines shown in Figure 14. The average load-transfer rate appeared to remain unchanged between stages. Finally, it is also important to mention that some points of stages 3 and 4 in Figure 14 situate above the 1:1 line, which means that the measured load exceeded the applied load, as a result of residual load build-up.
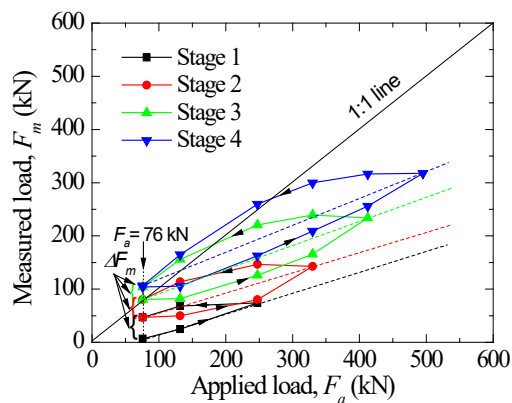
Figure 14 - Measured load at instrumented section SG1 as a function of the applied load at the anchor head.

Rev. IBRACON Estrut. Mater., vol. 14, no. 6, e14612, 2021

11/19

Figure 15 compares the load distribution obtained from the acceptance tests on the instrumented anchors with results from other experimental investigations [15], [16], [28]. Despite the differences in soils and retaining wall systems, it is noted that the responses of the anchors agree well with the previously published results. All results indicate that more than 50% of the axial load in the bonded length is dissipated within a length L_{se} equal to 0.4 L_b. However, in some anchors, the load dropped to less than 20% of the applied load within the same length, as shown by the response of anchor T33 and by the results from Briaud et al. [16].
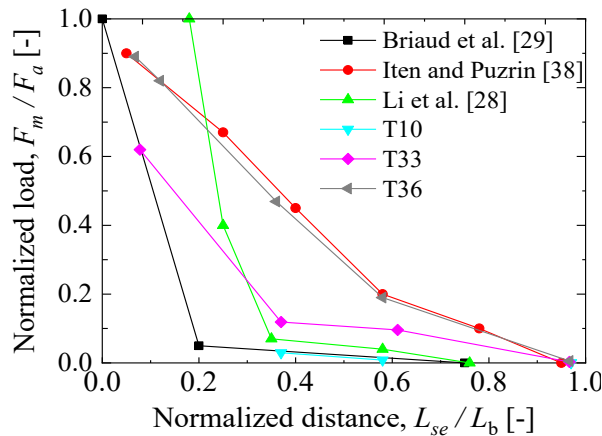
Figure 15 - Load distributions in the bonded length of the instrumented anchors compared with results reported in the literature.

4.3 Skin friction development on unbonded length of anchor T33

Figure 16 shows the skin friction on the unbonded length (f_{su}) as a function of the applied load (F_a), during the loading stages of the suitability test performed on ground anchor T33. Skin friction values were estimated from Equation 2. This analysis assumed that the skin friction develops uniformly along the unbonded length and that the load measured at the first instrumented section of the bonded length (SG1) equals that at the transition section between unbonded and bonded lengths. Also, the coefficient of diameter expansion in the unbonded length, $β$, was set equal to unity.

$$f_{su} = \frac{\left(F_a - F_{m(1)}\right)}{\pi \cdot \beta \cdot D_b \cdot L_u} \tag{2}$$

where $F_{m(1)}$ is the load measured at section SG1 (the other parameters were defined previously).

Figure 16 reveals a significant skin friction mobilization on the anchor unbonded length with increasing applied load. The skin friction was found to increase with increasing F_a, but at a reduced rate. Additionally, the skin friction became smaller at each new loading stage for the same applied load. For instance, the calculated skin friction for F_a = 132 kN varied from 68.2 kPa in load stage 1 to 16.9 kPa in load stage 4. This behavior took place due to the progressive transfer of stresses from the unbonded length to the bonded length between loading stages. The skin friction reached approximately the same maximum value (f_{max}) in all four loading stages, around 115 kPa, which can be assumed as the unbonded length ultimate skin friction $(f_{ult,u})$.

Figure 16 also reveals the occurrence of negative skin friction for F_a = 76 kN in loading stages 3 and 4. As the tensile load decreased after unloading, the anchor unbonded length recovered a portion of the elastic elongation. This rebound caused enough displacement to mobilize residual stresses at the bonded length (at least in the zone comprising the beginning of the bonded length) and reverse the skin friction direction at the unbonded length.
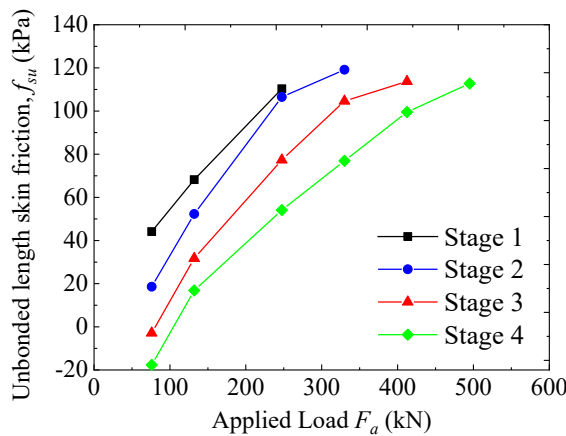
Figure 16 - Calculated skin friction on the unbonded length of ground anchor T33 during loading stages of the suitability test.

4.4 Skin friction development on bonded length of anchor T33

The skin friction on the bonded length (f_{sb}) of anchor T33, between instrumented sections, was estimated using Equation 3. The coefficient of diameter expansion in the bonded length, β, was assumed equal to 1.15 for this analysis.

$$f_{sb} = \frac{\left(F_{m(i)} - F_{m(i+1)}\right)}{\pi \cdot \beta \cdot D_b \cdot \left(L_{se(i)} - L_{se(i+1)}\right)} \tag{3}$$

where: $F_{m(i)}$ is the measured load at instrumented section SG_i; $F_{m(i+1)}$ is the measured load at instrumented section $SG_{(i+1)}$; $L_{se(i)}$ is the distance from the bonded length beginning to instrumented section SG_i; $L_{se(i+1)}$ is the distance from the bonded length beginning to instrumented section $SG_{(i+1)}$. L_{se} values are listed in Table 2 (Section 3.3).

Figure 17 presents the bonded length skin friction f_{sb} mobilized between sections SG1 and SG2, as a function of the applied load (F_a), during the four loading stages of the suitability test on anchor T33. The mobilized bonded length skin friction increased with F_a according to an increasing rate in loading stages 1 to 3, and according to an approximately constant rate in loading stage 4. In opposition, the skin friction followed a decreasing rate on the anchor's unbonded length, as shown in Figure 16. Also, contrary to what was found for the unbonded length, the skin friction in the bonded length increased after each new loading stage. Results presented in Figure 17 indicate that the ultimate skin friction (f_{ult}) at the bonded length was not reached for load range applied to the anchor head, since a tendency of stabilization of f_{sb} was not observed.
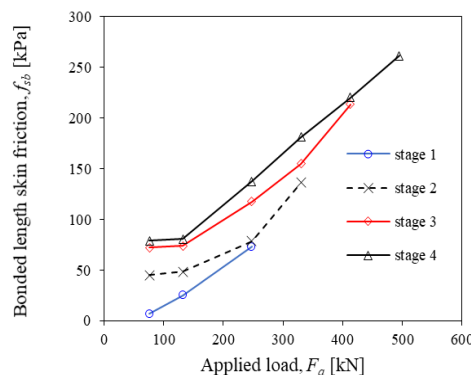
Figure 17 - Skin friction calculated between instrumented sections SG1 and SG2 of anchor T33 as a function of the applied load F_a.

Figure 18a-d shows the mobilized skin friction distribution along the bonded length of anchor T33 in the four loading stages of the suitability test. Mobilized skin friction values on the unbonded length are also included for comparison. Positions shown in Figure 18a-d were calculated from the anchor head to the midpoint between the anchor head and instrumented section SG1, and from the anchor head to the midpoint between each other instrumented section.

The skin friction was larger at the region of the bonded length closest to the transition between unbonded and bonded lengths. However, application of subsequent loading stages promoted a continuing transfer of stresses from the unbonded length to the bonded length, resulting in higher skin friction reaching the initial portion of the bonded length. At the first loading stage, the skin friction mobilized on the unbonded length was larger than that on the bonded length. Eventually, from the second loading stage, the skin friction on the bonded length superseded that on the unbonded length and concentrated almost completely at the initial half of the bonded length.

The important contribution of the anchor unbonded length to the overall pullout capacity of the anchor is clearly shown in Figure 18. It is observed that the unbonded length ultimate skin friction $\left(f_{ult,u}=115\,kPa\right)$ was mobilized since the first loading stage (Figure 18a). After $f_{ult,u}$ was reached in the first stage (Figure 18a), the mobilized skin friction in the following stages reduced on the unbonded length and intensified on the bonded length, at the same applied load F_a (Figure 18b,c,d). Ultimately, it is noted from the presented data that carrying out loading-unloading stages on the ground anchor intensified the transfer of load from the unbonded length to the bonded length. Thus, conducting acceptance pullout tests before lock-off, which include the application of loading-unloading stages, is beneficial for improving the bonded length skin friction and reducing the unbonded length skin friction. Such procedure is in line with most design codes and guidelines [25], [26], [37], [38].
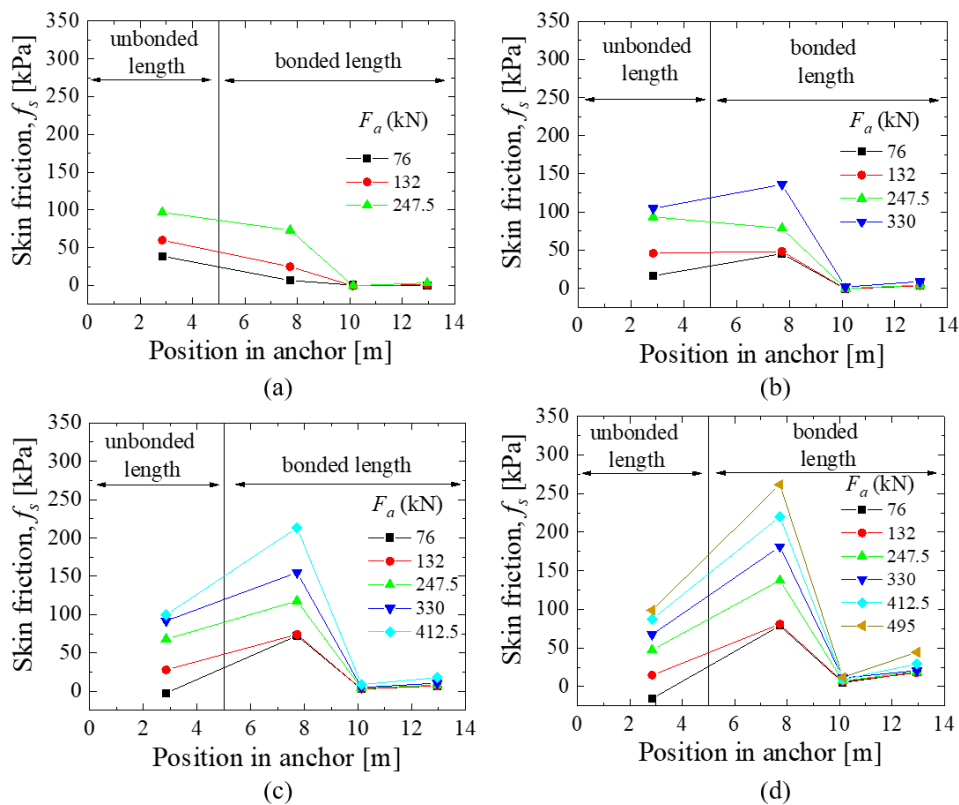
Figure 18 - Skin friction distribution on anchor T33: (a) 1st loading stage; (b) 2nd loading stage; (c) 3rd loading stage; (d) 4th loading stage.

It is important to emphasize that the shear resistance on the unbonded length shown in Figure 18 took place because of the way the anchors were jacked against the retaining wall. In the anchored wall system, the force in the anchor is generated by the active wedge moving towards the excavation, and the portion of the anchor within this zone will not

contribute to the system's stability. Therefore, the contribution of the anchor's unbonded length must not be taken into consideration in the design of anchored retaining walls. Instead, the contribution from the unbonded zone must be accounted for in the interpretation of a conventional pullout test result when the force is applied by jacking against the wall, so as not to overestimate the anchor capacity of the bond zone.

4.5 Comparison between experimental and predicted skin friction

Figure 19 compares the bonded length ultimate skin friction obtained from the field data collected from anchors T33 and T36 ($f_{ult,b,field}$) and with results obtained with the methods of Bustamante and Doix [22], Costa Nunes [7], ABNT NBR 5629 [24], AASHTO [23] and Ostermayer [3] ($f_{ult,b,pred}$). Anchor T10 was excluded from this analysis because its first instrumented section (SG1) was damaged during installation, which prevented obtaining the maximum mobilized skin friction on the bonded length (see Section 3.3). Since stabilization of f_{sb} with the applied load F_a was not achieved for anchor T33, as shown in Figure 17, the field ultimate skin friction was assumed equal to the maximum skin friction ($f_{ult,b,field} = f_{max}$).

Soil parameters were estimated based on the results of the field and laboratory tests (Section 3.3). Specifically, calculations were carried out by assuming that the soil unit weight equals 17 kN/m³ at the depth of the midpoint of the anchor upper row's bonded length and 18 kN/m³ at the depth of the midpoint of the anchor lower row's bonded length. Additionally, the soil effective internal friction angle and effective cohesion were assumed equal to 31° and 0 kPa, respectively.

The vertical stress increase due to the residual injection pressure (Δp) in Costa Nunes' [7] approach was considered equal to $5\gamma h$, as recommended by the author. However, it has been observed that this suggestion typically leads to predicted bearing capacity values much higher than those found in the field [20]. Thus, an additional prediction with Costa Nunes' [7] approach was carried out using $\Delta p = 0$ kPa.

The diameter increase of the bonded length due to the grouting process injection was assumed equals to 1.15 D_b in the methods of Bustamante and Doix [22], Costa Nunes [7], ABNT NBR 5629 [24] and AASHTO [23]. The anchorage coefficient (k_f) required in the method by ABNT NBR 5629 [24] was defined as 1.2, based on soil type.
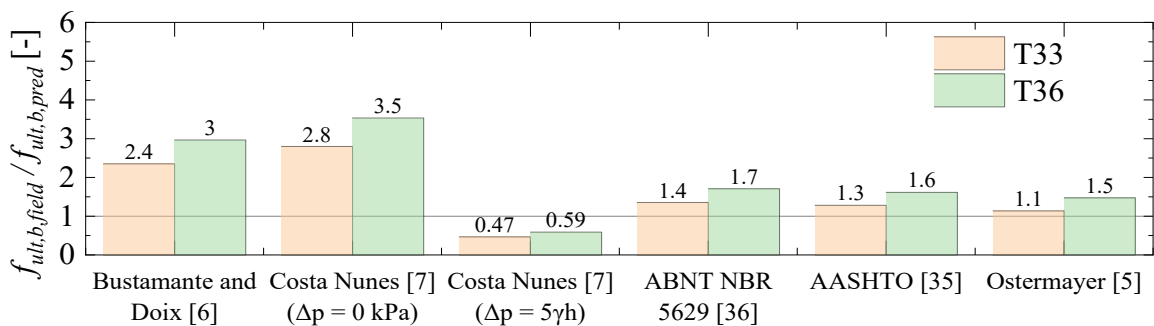
Figure 19 - Comparison between field and predicted ultimate skin friction on bonded length of anchors T33 and T36.

Figure 19 shows that the methods of Bustamante and Doix [22] and Costa Nunes [7] with $\Delta p = 0$ kPa provided over-conservative predictions. On the other hand, slightly conservative predictions were obtained with the methods by AASHTO [25], ABNT NBR 5629 [24] and Ostermayer [3]. On the other hand, predictions with Costa Nunes' [7] method with $\Delta p = 5\gamma h$ overestimated the pullout capacity by more than twice. Porto [20] warns about exaggerated results with this method when the vertical stress increase due to the residual injection pressure is taken into consideration.

All design methods assessed in Figure 19 assume that the skin friction mobilized on the bonded length of a ground anchor follows a uniform distribution [3], [7], [22]–[24]. Although the progressive failure mechanism (i.e., f_{ult} dropping off to the residual value after reaching peak) was not possible to be observed with the field tests, an indication of such behavior can be assessed from the experimental data presented in Figure 18. It may be noted that predictions

for pullout field tests could be improved with design methods that incorporate non-uniform skin friction distributions, in which the skin friction concentrates more at the first half of the anchor bonded length.

4.6 Monitoring of anchor T36 after lock-off

While monitoring of anchors T10 and T33 has been discontinued after lock-off, anchor T36 was continuously tracked for 328 days after lock-off. Figure 20 shows the variation of the load (F_m) measured in the instrumented sections during monitoring of anchor T36 (day 0 is when the anchor was locked-off). It can be observed that minor variations of load took place initially and equilibrium was reached in the long-term. These results are consistent with the findings of [18]. Particularly, the measured load in the bonded length of anchor T36 decreased with time at Sections SG1 to SG4 and increased slightly at section SG5. The most significant load relief took place five days after lock-off and was sharper at section SG1, which recorded a relief of about 11%. In the first minute after lock-off, the measured load at SG1 decreased by 5%. A similar tendency, though less pronounced, occurred at sections SG2 and SG3. The total relief of load at SG1 after 328 days was about 18% (7% of which occurred after the first 5 days). The load relief at SG2 and SG4 was about 7% and 4% after 328 days of installation, respectively. At the same time, the measured load increased slightly at section SG5. Once more, most of the load increase at SG5 occurred immediately after lock-off. No significant changes in the measured load were noticed during or after the third excavation phase of the retaining wall.

The load relief in the anchor bonded length in the long-term can be explained by the viscous behavior of the anchor components (grout, tendon, connections, etc.) and the surrounding soil [15], [39], [40]. A small portion of that load relief was transferred to the zone at the end of the bonded length.
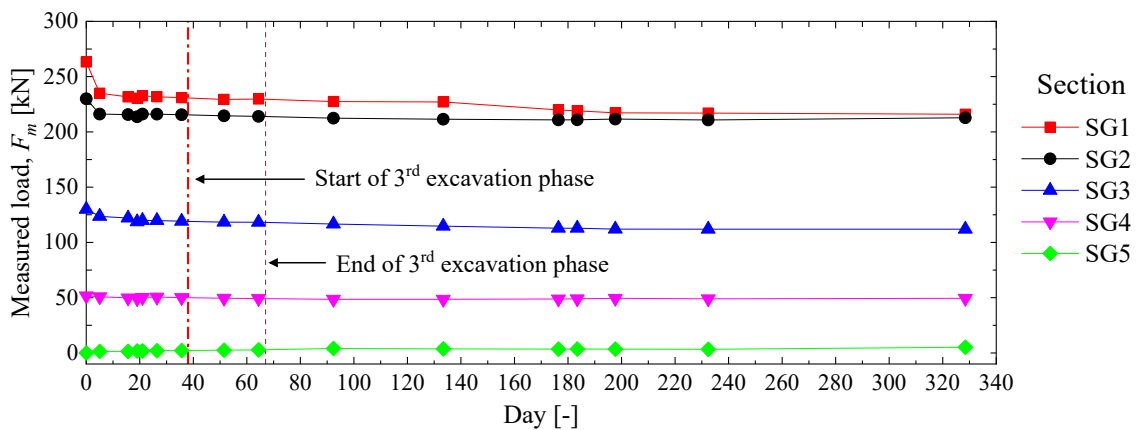
Figure 20 - Load monitoring along time for anchor T36.

5 CONCLUSIONS

This paper addresses the behavior of three instrumented prestressed ground anchors installed in a spaced bored pile retaining wall. The load in the ground anchors was measured with strain gauges installed in five distinct sections along the anchor bonded length. Load variations were monitored during pullout tests performed on the anchors, as well as along the different construction phases of the retaining wall system after locking-off. Skin friction mobilized on the anchor unbonded and bonded lengths were assessed from the data collected in the field. The following conclusions can be drawn from the experimental results obtained in this investigation:

(1) The measured load followed a non-uniform distribution along the anchor bonded length, being higher at the region closest to the beginning of the bonded length and dropping drastically within the farthest bonded length half. Residual load after anchor unloading was recorded close to the beginning of the anchor bonded length. Eventually, the residual load build-up caused the measured load to exceed the applied load after the anchor was submitted to a number of loading-unloading stages.

(2) The contribution of the unbonded length skin friction to the overall anchor capacity was found to be significant. The unbonded length skin friction increased at a reduced rate with increasing applied load and decreased with the application of the loading-unloading stages. Displacements applied to the anchor head were sufficient to mobilize

the ultimate skin friction on the unbonded length. Residual stresses in the bonded length caused the development of negative skin friction on the unbonded length after three loading-unloading stages.

(3) The field test results conducted in the present investigation show that the contribution from the unbonded length must be accounted for in the interpretation of conventional pullout test results so as not to overestimate the anchor capacity of the bonded length.

(4) The initial portion of the anchor bonded length experienced an increase in the mobilized skin friction after the application of loading-unloading stages on the anchor. The mobilized skin friction concentrated almost completely on the nearest bonded length half, while negligible skin friction was mobilized on the farthest bonded length half. The transfer of load from the unbonded length to the bonded length intensified after the ultimate skin friction on the unbonded length was achieved. Applied load levels were not sufficient to mobilize the ultimate skin friction on the anchor bonded length.

(5) Long-term monitoring after anchor lock-off revealed that, for the specific case of this project, the load in the anchor bonded length reduced slightly and then stabilized thereafter. The measured load was not significantly influenced by the retaining wall construction phases. Most load reliefs occurred within the first five days after lock-off. A discrete increase in the load with time was found near the end of the bonded length.

(6) Performance of loading-unloading stages on the ground anchor intensified the transfer of load from the unbonded length to the bonded length. The load transfer became more effective after the ultimate skin friction of the unbonded length was reached. Therefore, the required procedure in the design codes and guidelines for carrying out pullout tests, including loading-unloading stages during anchor installation before lock-off, appears to be well justified.

ACKNOWLEDGEMENTS

REFERENCES

[1] S. Yoshida, K. Komura, T. Matsumoto, and T. Yoshida, "Pull-out experiment of two-dimensional model flip-type ground anchors installed in dry sand ground," in *Geotechnics for Sustainable Infrastructure Development* (Lecture Notes in Civil Engineering, 62), P. D. Long and N. T. Dung, Eds., Switzerland: Springer, 2020, pp. 1245–1252.

[2] A. Parsapajouh, S. Litkouhi, and B. Amini, "A case study on excavation stabilization using ground anchors and high pressure injection," in *Proc. 4th Int. Conf. Grout. Deep Mix.*, New Orleans, Aug. 2012, pp. 1115–1123, http://dx.doi.org/10.1061/9780784412350.0092.

[3] H. Ostermayer, "Construction carrying behaviour and creep characteristics on ground anchors," in *Proc. Conf. Diaphragm Walls and Anchorages*, 1975, pp. 141–151, http://dx.doi.org/10.1680/dwaa.00056.0023.

[4] N. N. Thanh and N. P. Duy, "Full-scale pullout testing of ground anchors to evaluate the applicability of french design practice TA95 for Vietnam," in *CIGOS 2019, Innovation for Sustainable Infrastructure* (Lecture Notes in Civil Engineering 54), C. Ha-Minh, D. Van Dao, F. Benboudjema, S. Derrible, D. V. K. Huynh, and A. M. Tang, Eds., Switzerland: Springer, 2020, pp. 787–792.

[5] J.-L. Briaud and Y. Lim, "Tieback walls in sand: numerical simulation and design implications," *J. Geotech. Geoenviron. Eng.*, vol. 125, no. 2, pp. 101–110, Feb 1999, http://dx.doi.org/10.1061/(ASCE)1090-0241(1999)125:2(101).

[6] F. Rashidi and H. Shahir, "Numerical investigation of anchored soldier pile wall performance in the presence of surcharge," *Int. J. Geotech. Eng.*, vol. 13, no. 2, pp. 162–171, Mar 2019, http://dx.doi.org/10.1080/19386362.2017.1329258.

[7] A. J. Costa Nunes, "Ground prestressing: first casagrande lecture," in *VIII CPAMSEF*, Cartagena, Colombia, 1987.

[8] I. O. Joppert Jr., W. Mallmann, and W. R. Iorio, "Calculation method for estimation of failure load in self-perforating tie-backs of tubular type," in *Sem. Eng. de Fund. Esp. Geotec. SEFE V*, São Paulo, 2004.

[9] M. Yazdandoust, "Seismic performance of soil-nailed walls using a 1g shaking table," *Can. Geotech. J.*, vol. 55, no. 1, pp. 1–18, 2018, http://dx.doi.org/10.1139/cgj-2016-0358.

[10] G. Zhang, J. Cao, and L. Wang, "Centrifuge model tests of deformation and failure of nailing-reinforced slope under vertical surface loading conditions," *Soil Found.*, vol. 53, no. 1, pp. 117–129, Feb 2013, http://dx.doi.org/10.1016/j.sandf.2012.12.008.

[11] H. Arefizadeh and H. Shahir, "Three-dimensional analysis of anchored wall with concrete bearing pads," *J. Eng. Des. Technol.*, vol. 18, no. 6, pp. 1469–1486, Jan 2020, http://dx.doi.org/10.1108/JEDT-09-2019-0229.

[12] R. Moffat, P. Parra, and M. Carrasco, "Monitoring a 28.5 m high anchored pile wall in gravel using various methods," *Sens. Switz.*, vol. 20, no. 1, pp. 80, Dec 2020, http://dx.doi.org/10.3390/s20010080.

[13] K. Gorska and M. Wyjadłowski, "Analysis of displacement of excavation based on inclinometer measurements," *Stud. Geotech. Mech.*, vol. XXXIV, no. 4, pp. 3–16, 2012, http://dx.doi.org/10.2478/sgm041201.

[14] R. J. Finno and J. F. Roboski, "Three-dimensional responses of a tied-back excavation through clay," *J. Geotech. Geoenviron. Eng.*, vol. 131, no. 3, pp. 273–282, Mar 2005, http://dx.doi.org/10.1061/(ASCE)1090-0241(2005)131:3(273).

[15] J. C. Li, H. L. Yao, L. P. Shi, and B. I. Shy, "Behavior of ground anchors for Taipei sedimentary soils," in *Proc. 2nd Int. Conf. Case Histories Geotec. Eng.* (Paper No. 6.73), 1988.

[16] J. L. Briaud, A. Y. Griffin, A. Soto, A. Suroor, and H. Park, *Long-Term Behavior of Ground Anchors and Tieback Walls, Report FHWA_1391-1.* Texas: Department of Transportation, 1998.

[17] X. Liu, J. Wang, J. Huang, and H. Jiang, "Full-scale pullout tests and analyses of ground anchors in rocks under ultimate load conditions," *Eng. Geol.*, vol. 228, pp. 1–10, Oct 2017, http://dx.doi.org/10.1016/j.enggeo.2017.07.004.

[18] L. S. Bryson and J. R. Giraldo, "Analysis of case study presenting ground anchor load-transfer response in shale stratum," *Can. Geotech. J.*, vol. 57, no. 1, pp. 85–99, Jan 2020, http://dx.doi.org/10.1139/cgj-2018-0326.

[19] B. Benmokrane, M. Chekired, and H. Xu, "Monitoring behavior of grouted anchors using vibrating-wire gauges," *J. Geotech. Eng.*, vol. 121, no. 6, pp. 466–475, 1995, http://dx.doi.org/10.1061/(ASCE)0733-9410(1995)121:6(466).

[20] T. B. Porto, "Anchors in soils - geotechnical behavior and methodology web for prediction and control," Ph.D. dissertation, Grad. Program Geotech., Univ. Fed. Ouro Preto, Ouro Preto, 2015.

[21] M. Turner, "Geotechnical design of ground anchors," in *ICE Manual of Geotechnical Engineering Volume II - Geotechnical Design, Construction and Verification*, J. Burland, T. Chapman, H. Skinner and M. Brown, Eds., ICE Publishing, 2012, pp. 1011.

[22] M. Bustamante and B. Doix, "Une méthode pour le calcul des tirants et des micropieux injectés," *Bull. Liaison des Lab. Ponts Chaussees*, no. 140, pp. 75–92, 1985.

[23] American Association of State Highway and Transportation Officials, *AASHTO LRFD Bridge Design Specifications*, 8th ed., 2017.

[24] Associação Brasileira de Normas Técnicas, *Procedure of Ties Anchored in Soil*, ABNT NBR 5629, 2006.

[25] Canadian Geotechnical Society, *Canadian Foundation Engineering Manual.* Ottawa: CGS, 2006.

[26] Associação Brasileira de Normas Técnicas, *Ties Anchored in Soil – Design and Execution*, ABNT NBR 5629:2018, 2018.

[27] M. Iten and A. M. Puzrin, "Monitoring of stress distribution along a ground anchor using BOTDA," *Sensors Smart Struct. Technol. Civil, Mech. Aerosp. Syst.*, vol. 7647, pp. 1–15, 2010, http://dx.doi.org/10.1117/12.847499.

[28] N.-K. Kim, "Performance of tension and compression anchors in weathered soil," *J. Geotech. Geoenviron. Eng.*, vol. 129, no. 12, pp. 1138–1150, Dec 2003, http://dx.doi.org/10.1061/(ASCE)1090-0241(2003)129:12(1138).

[29] N. Moraci and P. Recalcati, "Factors affecting the pullout behaviour of extruded geogrids embedded in a compacted granular soil," *Geotext. Geomembr.*, vol. 24, no. 4, pp. 220–242, Aug 2006, http://dx.doi.org/10.1016/j.geotexmem.2006.03.001.

[30] K. Fujita, K. Ueda, and M. Kusabuka, "A method to predict the load-displacement relationship of ground anchors," *Rev. Fr. Geotechnique*, vol. 1, no. 3, pp. 58–62, Oct 1978, http://dx.doi.org/10.1051/geotech/1978003058.

[31] A. D. Barley and C. R. Windsor, "Recent advances in ground anchor and ground reinforcement technology with reference to the development of the art," in *Proc. Int. Conf. Geotech. Geol. Eng.*, 2000.

[32] K. M. Platzer, C. Wendeler, R. Brändle, and M. Stolz, "Experimental investigation of forces along anchors subjected to dynamic loading under tension and compression in field tests," *Can. Geotech. J.*, vol. 57, no. 5, pp. 770–782, May 2020, http://dx.doi.org/10.1139/cgj-2018-0144.

[33] Associação Brasileira de Normas Técnicas, *Soil - Standard Penetration Test - SPT - Soil Sampling and Classification - Test Method*, ABNT NBR 6484:2001, 2001.

[34] L. Décourt, A. Belincanta, and A. Quaresma Fo., "Brazilian experience on SPT," in *Suppl. Contrib. Braz. Soc. Soil Mech., XII ICSMFE*, 1989, pp. 49–54.

[35] A. B. Cerato and R. Victor, "Effects of long-term dynamic loading and fluctuating water table on helical anchor performance for small wind tower foundations," *J. Perform. Constr. Facil.*, vol. 23, no. 4, pp. 251–261, Aug 2009., http://dx.doi.org/10.1061/(ASCE)CF.1943-5509.0000013.

[36] J. A. Schiavon, C. H. C. Tsuha, A. Neel, and L. Thorel, "Centrifuge modelling of a helical anchor under different cyclic loading conditions in sand," *Int. J. Phys. Model. Geotech.*, vol. 19, no. 2, pp. 72–88, Mar 2019, http://dx.doi.org/10.1680/jphmg.17.00054.

[37] British Standards Institution, *Code of Practice for Grouted Anchors*, BSI 8081:2015, 2015.

[38] A. R. Gaba, B. Simpson, W. Powrie, and D. R. Beadman, *Embedded Retaining Walls: Guidance for Economic Design* (CIRIA Report, C580). London: GB. Constr. Ind. Res. Inf. Assoc., 2003.

[39] A. Correia, A. G. Guerra, and N. C. Pinto, "Behavior of three retaining wall structures of Berlin type," *Geotec. Rev. Soc. Port. Geotec.*, vol. 1, no. 81, pp. 65–78, 1996.

[40] S. W. Choi, J. Lee, J. M. Kim, and H. S. Park, "Design and application of a field sensing system for ground anchors in slopes," *Sensors*, vol. 13, no. 3, pp. 3739–3752, 2013, http://dx.doi.org/10.3390/s130303739. PMid:23507820.

[41] M. H. Baziar, A. Ghadamgahi, and A. J. Brennan, "Numerical analysis of collapse in a deep excavation supported by ground anchors," *Proc. Inst. Civ. Eng. Geotech. Eng.*, pp. 1–45, 2020, http://dx.doi.org/10.1680/jgeen.19.00122.

[42] A. Ahmadi and M. M. Ahmadi, "Three-dimensional numerical analysis of corner effect of an excavation supported by ground anchors," *Int. J. Geotech. Eng.*, pp. 1–13, Oct. 2019, http://dx.doi.org/10.1080/19386362.2019.1682349.

[43] N. K. Kim, J. S. Park, and S. K. Kim, "Numerical simulation of ground anchors," *Comput. Geotech.*, vol. 34, no. 6, pp. 498–507, Nov 2007, http://dx.doi.org/10.1016/j.compgeo.2006.09.002.

[44] H. Y. Xu, L. Z. Chen, and J. L. Deng, "Uplift tests of jet mixing anchor pile," *Soil Found.*, vol. 54, no. 2, pp. 168–175, Apr 2014, http://dx.doi.org/10.1016/j.sandf.2014.02.008.

[45] B. V. S. Viswanadham and V. M. Rotte, "Effect of facing type on the behaviour of soil-nailed slopes: centrifuge and numerical study," *Discovery*, vol. 46, no. 215, pp. 214–223, 2015. Accessed: Dec. 07, 2020. [Online]. Available: www.discoveryjournals.com

[46] W. B. Wei and Y. M. Cheng, "Soil nailed slope by strength reduction and limit equilibrium methods," *Comput. Geotech.*, vol. 37, no. 5, pp. 602–618, Jul 2010, http://dx.doi.org/10.1016/j.compgeo.2010.03.008.

[47] D. P. Deng, L. Li, and L. H. Zhao, "Limit equilibrium analysis for stability of soil nailed slope and optimum design of soil nailing parameters," *J. Cent. South Univ.*, vol. 24, no. 11, pp. 2496–2503, Nov 2017, http://dx.doi.org/10.1007/s11771-017-3662-y.

[48] S. Rawat and A. K. Gupta, "Analysis of a nailed soil slope using limit equilibrium and finite element methods," *Int. J. Geosynth. Gr. Eng.*, vol. 2, no. 4, pp. 1–23, Dec 2016, http://dx.doi.org/10.1007/s40891-016-0076-0.

[49] S. K. Razavi and M. Hajialilue Bonab, ""Study of soil nailed wall under service loading condition," *Proc. Inst. Civ. Eng. Geotech. Eng.*, vol. 170, no. 2, pp. 161–174, Apr 2017, http://dx.doi.org/10.1680/jgeen.16.00006.

[50] G. Zhang, J. Cao, and L. Wang, "Failure behavior and mechanism of slopes reinforced using soil nail wall under various loading conditions," *Soil Found.*, vol. 54, no. 6, pp. 1175–1187, Dec 2014, http://dx.doi.org/10.1016/j.sandf.2014.11.011.

[51] P. J. Sabatini, D. G. Pass, and R. C. Bachus, *Ground Anchors and Anchored Systems*, 4th ed. (Geotechnical Engineering Circular). Washington: Assoc. Drilled Shaft Contract. (U.S.), GeoSyntec Consult., Fed. Highw. Adm., Off. Bridge Technol., 1999.

[52] R. I. Woods and K. Barkhordari, "The influence of bond stress distribution on ground anchor design," in *Gr. Anchorages Anchored Struct. Proc. Conf. London*, 1997, pp. 55–64.